

Modelling the spatial shape of nondiffracting beams: experimental generation of Frozen Waves via holographic method ^(†)

Tárcio A. Vieira ⁽¹⁾, Michel Zamboni-Rached ⁽²⁾ and Marcos R.R. Gesualdi ⁽³⁾

^(1,3) *Universidade Federal do ABC, Santo André, SP, Brazil.*

⁽²⁾ *University of Campinas, Campinas, SP, Brazil.*

Abstract – In this paper we implement experimentally the spatial shape modelling of nondiffracting optical beams via computer generated holograms on spatial light modulators. The results reported here are the experimental confirmation of the so called Frozen Wave method, developed few years ago. Optical beams of this type can possess potential applications in optical tweezers, medicine, atom guiding, remote sensing, etc..

1 Introduction

Few years ago, in a series of papers [1, 2, 3, 4], an interesting theoretical method was developed, capable to furnish nondiffracting beams whose longitudinal intensity shape can be freely chosen a priori.

This approach is based on suitable superposition of equal frequency and co-propagating Bessel beams, and the resulting wave fields are called Frozen Waves* (FWs). Besides a strong control on the longitudinal intensity pattern, this method also allows a certain control on the transverse shape of the resulting beam.

Due to their unique characteristics, i.e., their nondiffracting and spatial modelling properties, the FWs are quite interesting for many applications such as optical tweezers, remote sensing, atom guiding, medical purposes, etc. [5, 6, 7]

Very recently [8] the FW method was experimentally verified through the experimental generation by holographic method of few FWs previously chosen.

^(†) E-mail addresses for contacts: mzamboni@dmo.fee.unicamp.br

*This approach is also called *Frozen Wave method*

In this paper we shall present the experimental generation of several new and very interesting FWs through the implementation of amplitude computer generated holograms (CGHs) in spatial light modulators (SLMs). Our results confirm, once more, the theoretical predictions of the method developed in [1, 2], and open exciting possibilities on the applicability of these very especial beams.

In the next section we make a synthesis of the theoretical FW method. After this, in section 3, we show the experimental results concerning to the generation of several nondiffracting beams whose spatial shape were previously chosen. The experimental generation is made by amplitude computer generated holograms implemented in two types of spatial light modulators, transmission and reflective.

2 Summarizing the theoretical Frozen Wave method

The theory of FWs was formulated in [1] and further improved in [2, 3, 4].

Here we shall summarize the method without entering into the mathematical details, which can be found in the references above.

Trying to be brief, what we wish is to construct exact solutions of the wave equation representing nondiffracting beams whose the longitudinal intensity pattern, $|F(z)|^2$, in the interval $0 \leq z \leq L$, can be freely chosen a priori.

This can be done by considering a superposition of equal frequency and co-propagating Bessel beams of order ν :

$$\Psi(\rho, \phi, z, t) = e^{-i\omega t} \sum_{n=-N}^N A_n J_\nu(k_{\rho n} \rho) e^{ik_{zn} z} e^{i\nu\phi} \quad (1)$$

with

$$k_{\rho n}^2 = k^2 - k_{zn}^2 \quad (2)$$

where k , $k_{\rho n}$ and k_{zn} , are the total, the transverse and the longitudinal wave numbers respectively of the nth Bessel beam in the superposition 1.

In expression (1) the following choice is made:

$$k_{zn} = Q + 2\pi n/L \quad (3)$$

where Q is a constant such that

$$0 \leq Q + (2\pi/L)n \leq \omega/c \quad (4)$$

for $-N \leq n \leq N$.

The condition given by (4) ensures forward propagation only, with no evanescent waves. The constant parameter Q can be freely chosen, provided that (4) be obeyed, and it plays an important role in determining the spot size of the resulting beam.

Still considering Eq.(1), we adopt the following choices for the coefficients A_n :

$$A_n = \frac{1}{L} \int_0^L F(z) e^{-i\frac{2\pi}{L}nz} dz \quad (5)$$

where, as we said, $|F(z)|^2$ is the desired longitudinal intensity pattern in the interval $0 \leq z \leq L$.

Now, it is important to notice that this longitudinal intensity pattern can be concentrated, as we wish, over the propagation axis ($\rho = 0$) or over a cylindrical surface.

In the case we wish this intensity concentrated over the propagation axis, $\rho = 0$, zero order Bessel beams (i.e. $\nu = 0$) are to be used in the fundamental superposition (1). It is also possible to choose the spot radius, $\Delta\rho_0$, of the resulting beam by making $Q = (\omega^2/c^2 - 2.4^2/\Delta\rho_0^2)^{1/2}$.

Now, if we wish this intensity configuration concentrated over a cylindrical surface, so higher order Bessel beams, i.e. $\nu \geq 1$, are to be used in (1). In this case, the radius ρ_0 of the cylindrical surface can be approximately chosen if we pick up the value of Q as given by

$$\left[\frac{d}{d\rho} J_\nu \left(\rho \sqrt{\omega^2/c^2 - Q^2} \right) \right] \Big|_{\rho=\rho_0} = 0 \quad (6)$$

3 Experimental generation of Frozen Waves via holographic method

The use of spatial light modulators devices in holographic setups has become possible interesting applications in image phase correction, code signal encrypted and generation of optical beams [9, 10, 11, 12, 8, 13, 14].

The experiments conducted by us to generate interesting types of FWs are based on the holographic method. With the desired beams described by analytical exact solutions of the wave equation [15], we created an amplitude Computer Generated Holograms (CGH), which is reconstructed by a nematic liquid crystal spatial light modulator (LC-SLM).

More specifically, once we have chosen the desired beam spatial shape (i.e., the beam's longitudinal intensity pattern, $|F(z)|^2$, its spot radius or the radius of its cylindrical form), it can be approximately described by the analytical and exact FW solution (1,3,4,5). The amplitude CGH is constructed from the FW complex field $\Psi(\rho, \phi, z, t)$ (called FW-CGH) at the origin of the propagation direction, i.e. at ($z = 0$), and it is given by the following transmittance hologram equation,

$$H(x, y) = 1/2 \{ \beta(x, y) + \alpha(x, y) \cos[\phi(x, y) - 2\pi(\xi x + \eta y)] \} \quad (7)$$

where, $\alpha(x, y)$ and $\phi(x, y)$ are amplitude and phase of the FW complex field $\Psi(\rho, \phi, z, t)$, respectively. For reducing the noise of the signal spectrum hologram, the conventional bias function $\beta(x, y) = [1 + \alpha^2(x, y)]/2$ is taken as a soft envelope of the amplitude $\alpha(x, y)$ [12]. To separate different diffraction orders from the encoded complex field $\Psi(\rho, \phi, z, t)$, the off-axis reference plane wave $\exp[i2\pi(\xi x + \eta y)]$ is used. In Fourier plane, the center of signal information is shifted to values of spatial frequencies (ξ, η) and should be chosen according to diffraction efficiency and bandwidth of the SLM [11, 8].

To guarantee the efficient generation of the FW in the chosen interval, we have used (to the FW-CGH) a circular aperture of minimum diameter D given by

$$D_{min} \geq 2L \left[\left(\frac{k}{k_{zn=-N}} \right)^2 - 1 \right]^{1/2} \quad (8)$$

The parameters Q and L give us, via Eq.(4), the maximum number, $2N_{max} + 1$, of Bessel beams in the superposition (1). If we consider $Q > k/2$ (as usually occurs), so

$$N_{max} = [L(k - Q)/2\pi] \quad (9)$$

where $[.]$ is the floor function, i.e., N_{max} is the greatest integer less than or equal to $L(k - Q)/2\pi$.

3.1 Holographic experimental setups

In this work we have experimentally generated seven different and interesting FWs, in five of them it was used a transmission SLM, being the other two created with a reflective one. The most significant differences between them is the pixel resolution, and consequently, bandwidth and effective display area. We will see later the implications of this differences in holographic reconstruction processes of the FW complex field.

In the experimental holographic setups for FW generation, Fig.1(a) to transmission SLM (Setup 1) and Fig.1(b) to reflective SLM (Setup 2), we have a He-Ne laser (632.8nm) that is expanded and collimated (Exp) in a SLM device. Here we use the amplitude modulation with the polarizer Pol (angle 0°) and analyzer Anl (angle 90°) measured with respect to the input axis in the SLM. The 4-f spatial filtering system is used for FW experimental generation.

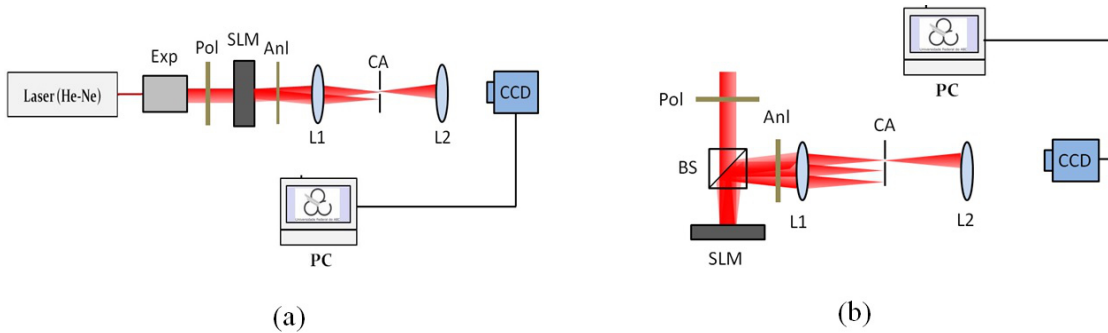


Figure 1: (a) experimental Setup 1 (b) experimental Setup 2, for FW generation, where SF is a spatial filter, L's are lenses, Pol is polarizer, Anl is analyzer, CA is a circular aperture mask, CCD is the camera. In (a) SLM is a LC2002 transmission SLM and (b) SLM is a LC-R1080 reflective SLM,

The transmission modulator used in setup 1 is the LC-2002 SLM model, Holoeye Photonics. It has an array of pixels (800×600) with each pixel measuring 32 micrometers, the shortest side of the display possesses 19,2mm and the bandwidth $\delta p = 3.1 \times 10^4 m^{-1}$.

The reflective SLM used in setup 2 is the LC-R1080 SLM model, Holoeye Photonics, that possesses each pixel measuring $8.1\mu m$ in a display matrix (1920×1200), the lowest edge with 9.7mm and the bandwidth $\delta p = 12.346 \times 10^4 m^{-1}$. Considering the limitations described above, this implies that the limit for the diameter of the CGH is approximately two times lower and bandwidth δp is four times higher compared to those of Setup 1.

In more detail, in both setups the LC-SLM (FW-CGH) is placed at the input plane (focus of lens $L1$) and, a spatial filtering mask (SF , band-pass circular pupil), at the Fourier plane, to select and transmits the shifted signal spectrum generating the FW field $\Psi(\rho, \phi, z)$ at the output plane of the setup. As a result, we have the propagation of the desired FW, whose intensity is registered with a CCD camera that can be displaced along the distance $0 \leq z \leq L$.

3.2 Results

The selection of parameters to be used in the experimental implementation for FW generation should consider the properties of the spatial light modulator that is being used. Two important parameters of the SLMs are limiting in this process: the bandwidth and the length of the shortest side of the SLM display. The first limitation is associated with the loss of information in the reconstruction process of the computer generated hologram (CGH); and, the second limitation is related to the diameter that the CGH (containing the complex field superposition) should possess in order to guarantee the efficient generation of the FW in the required spatial range $0 \leq z \leq L$.

We will discuss and compare the experimental results of FWs fields generated by holographic method using SLMs.

In the generation of the first five FWs below it was used the experimental setup 1, and in the last two the setup 2 was adopted. In all cases the procedure is the same: first, we choose the desired longitudinal intensity pattern, $|F(z)|^2$, for the nondiffracting beam;

after this, we use the solution (1) with k_{zn} and A_n given by Eqs. (3) and (5). The value of Q , and consequently the value of N_{max} , can be chosen through the desired beam spot size, or according to the resolution limit of the SLM. In solution (1), we use $\nu = 0$ or $\nu \geq 1$ depending if the desired longitudinal intensity pattern should be on the z axis or on a cylindrical surface, respectively.

The examples of FWs considered here are designed to furnish nondiffracting beams with interesting intensity patterns. For transmission SLM we use $Q = 0.9999943 k$, $N = 9$ and $L = 100$ cm. For reflective SLM we adopt $Q = 0.99996 k$, $N = 24$, and again $L = 100$ cm.

Unless otherwise stated, we will consider FWs generated from superpositions of zero-order Bessel beams, i.e., we will use $\nu = 0$ in the FW solution (1).

First and second examples of FWs:

Consider a couple of longitudinal intensity patterns, $|F(z)|^2$, in the range $0 \leq z \leq L$, given by a sequence of two and three unitary step functions, described by

$$F(z) = \begin{cases} 1, & \text{for } l_1 < z < l_2 \\ 1, & \text{for } l_3 < z < l_4 \\ 0, & \text{elsewhere} \end{cases} \quad (10)$$

$$F(z) = \begin{cases} 1, & \text{for } l_1 < z < l_2 \\ 1, & \text{for } l_3 < z < l_4 \\ 1, & \text{for } l_5 < z < l_6 \\ 0, & \text{elsewhere} \end{cases} \quad (11)$$

with $l_1 = 10$ cm, $l_2 = 40$ cm, $l_3 = 50$ cm, $l_4 = 60$ cm in Eq.10 and with $l_1 = 10$ cm, $l_2 = 20$ cm, $l_3 = 30$ cm, $l_4 = 50$ cm, $l_5 = 60$ cm, $l_6 = 70$ cm in Eq.11.

As it was said, we use the solution (1) with k_{zn} and A_n given by Eqs. (3) and (5). Now we have to choose the value of Q , which defines the spot size of the resulting FW and, together with L , determines N_{max} . Moreover, from the experimental point of view, it is very important to make an appropriated choice to Q in order to respect the resolution limit of the SLM. Concerning to this, and as a sufficient (but sometimes not necessary) condition, we should have the highest value of k_{pn} , given by $k_{pn=-N}$, limited by the bandwidth magnitude of the SLM.

Using $Q = 0.9999943 k$, we get $N_{max} = 9$ and a minimum diameter of $D = 9.55\text{mm}$, which is compatible with the dimensions of the SLM display. Finally, in this case we have $k_{\rho m=-N} = 4.74 \times 10^4 m^{-1}$, which respect the bandwidth of SLM.

In this case we have $k_{\rho m=0} = 3.3525 \times 10^4 m^{-1}$, which implies in a spot of radius $\Delta\rho_0 = 71.6 \mu\text{m}$ to the resulting FW.

Of course, the greater the number of terms in the series (1), the better the result, i.e., the resulting FW will be further closer to the desired beam.

The results, theoretical and experimental, are shown in Figures 2 and 3.

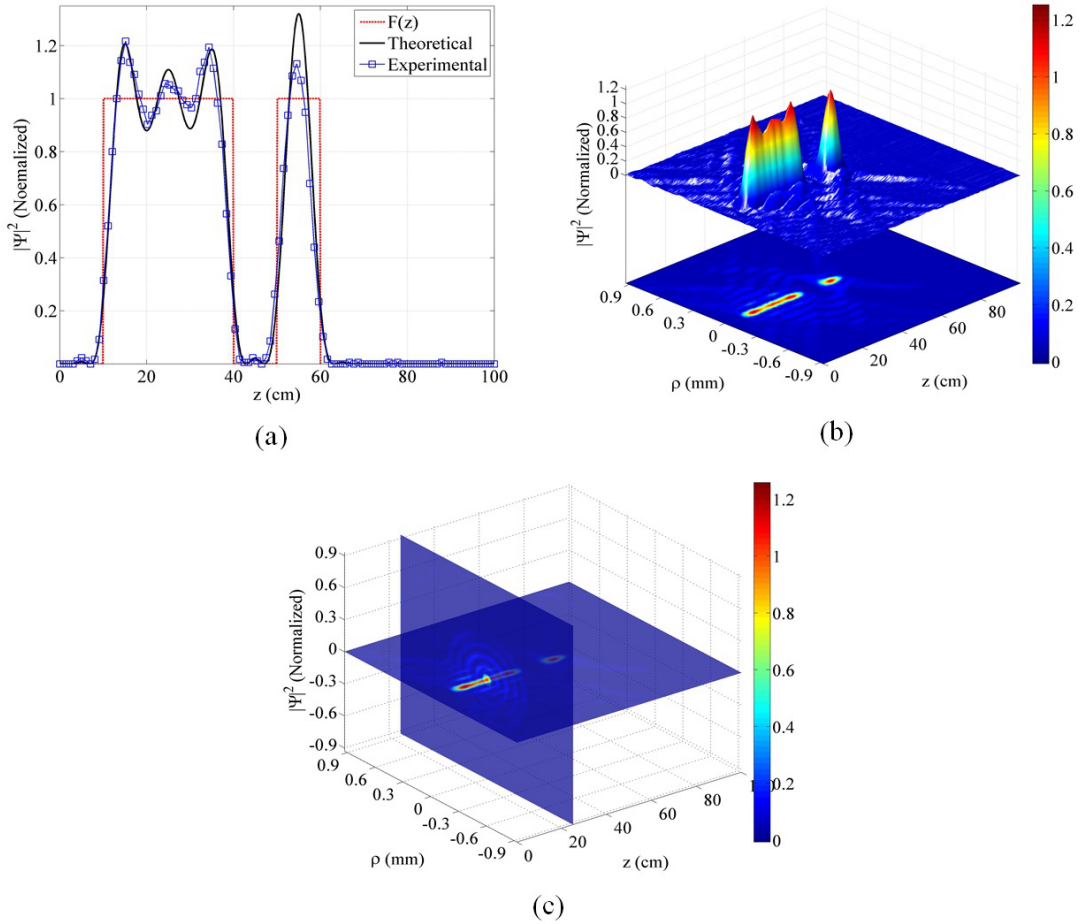
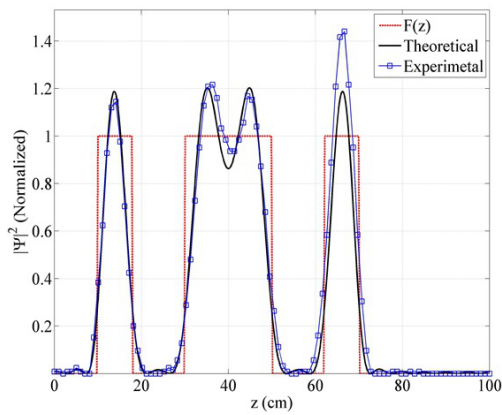
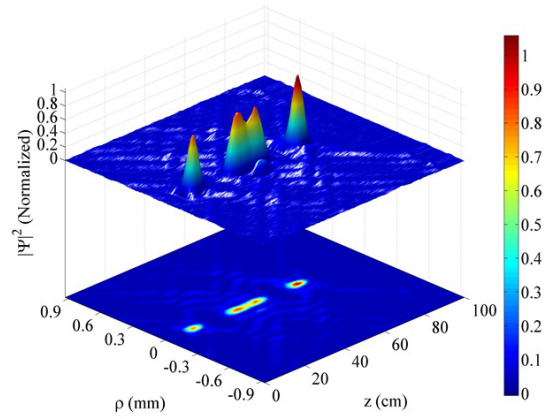


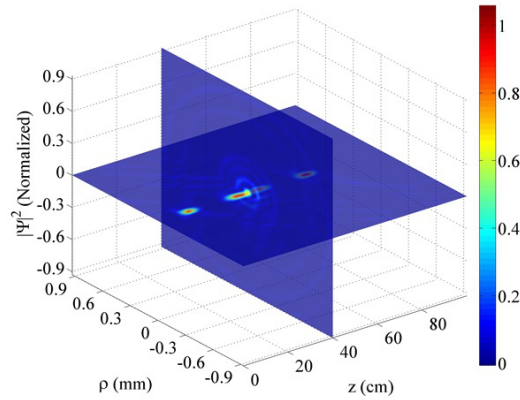
Figure 2: (a) Comparison among the longitudinal (on-axis) intensity patterns: $|F(z)|^2$, with $F(z)$ given by Eq.10, and the respective theoretical and experimental FWs; (b) Three-dimensional and projected shapes of the experimental FW; (c) Intensity pattern slices of the experimental FW.



(a)



(b)



(c)

Figure 3: (a) Comparison among the longitudinal (on-axis) intensity patterns: $|F(z)|^2$, with $F(z)$ given by Eq.11, and the respective theoretical and experimental FWs; (b) Three-dimensional and projected shapes of the experimental FW; (c) Intensity pattern slices of the experimental FW.

Figure 4 shows the comparison among the longitudinal projection intensity and transversal pattern for $|F(z)|^2$, given by Eq.(11), these results theoretical and experimental FW are in excellent agreement.

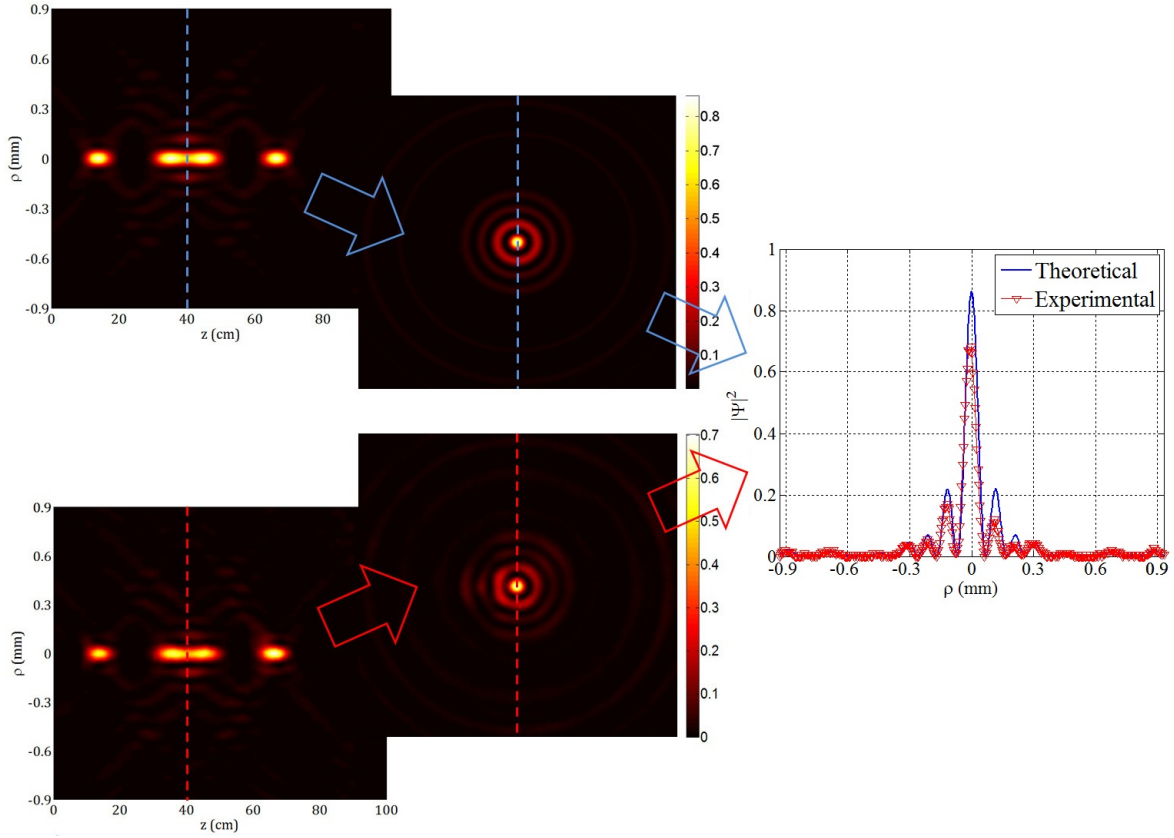


Figure 4: Comparison among the orthogonal projection and the transverse pattern of the intensities of the theoretical (up) and experimental (down) FWs with $F(z)$ given by Eq.(10).

It is easy to see that these FWs have nondiffracting properties, i.e., they resist to the diffraction effects for long distances. For instance, in example 1 we see an intensity and spot size invariance over 35 cm, while a gaussian beam with the same initial spot radius (of $71\mu\text{m}$) doubles its transverse width after 2.5 cm.

Third example:

Here we choose a ladder-shaped longitudinal intensity pattern, $|F(z)|^2$, being

$$F(z) = \begin{cases} 0.3, & \text{for } l_1 < z < l_2 \\ 0.6, & \text{for } l_2 < z < l_3 \\ 1, & \text{for } l_3 < z < l_4 \\ 0, & \text{elsewhere} \end{cases} \quad (12)$$

with $l_1 = 5\text{cm}$, $l_2 = 30\text{cm}$, $l_3 = 50\text{cm}$, $l_4 = 70\text{cm}$.

Figure 5 show the theoretical and experimental Frozen Waves obtained. We observe

an excellent agreement between them.

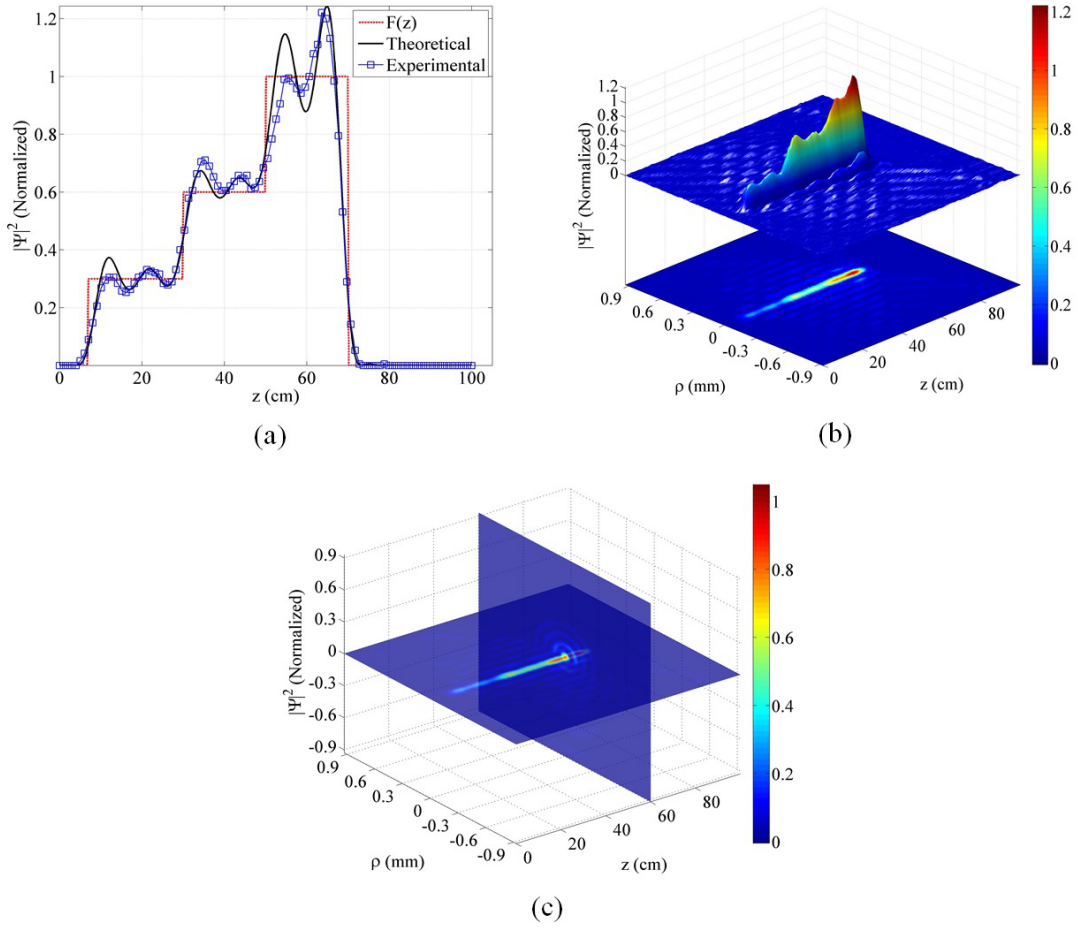


Figure 5: (a) Comparison among the longitudinal (on-axis) intensity patterns: $|F(z)|^2$, with $F(z)$ given by Eq.12, and the respective theoretical and experimental FWs; (b) Three-dimensional and projected shapes of the experimental FW; (c) Intensity pattern slices of experimental the FW.

Fourth example:

Another interesting case is a swab-shaped longitudinal intensity pattern. This can be reached by choosing

$$F(z) = \begin{cases} 1, & \text{for } l_1 < z < l_2 \\ 1/2, & \text{for } l_2 < z < l_3 \\ 1, & \text{for } l_3 < z < l_4 \\ 0, & \text{elsewhere} \end{cases} \quad (13)$$

whith, $l_1 = 10\text{cm}$, $l_2 = 20\text{cm}$, $l_3 = 60\text{cm}$, $l_4 = 70\text{cm}$.

Our results are shown in the Figure 6. Again, there is an excellent agreement between the theoretical FW ant that generated experimentally.

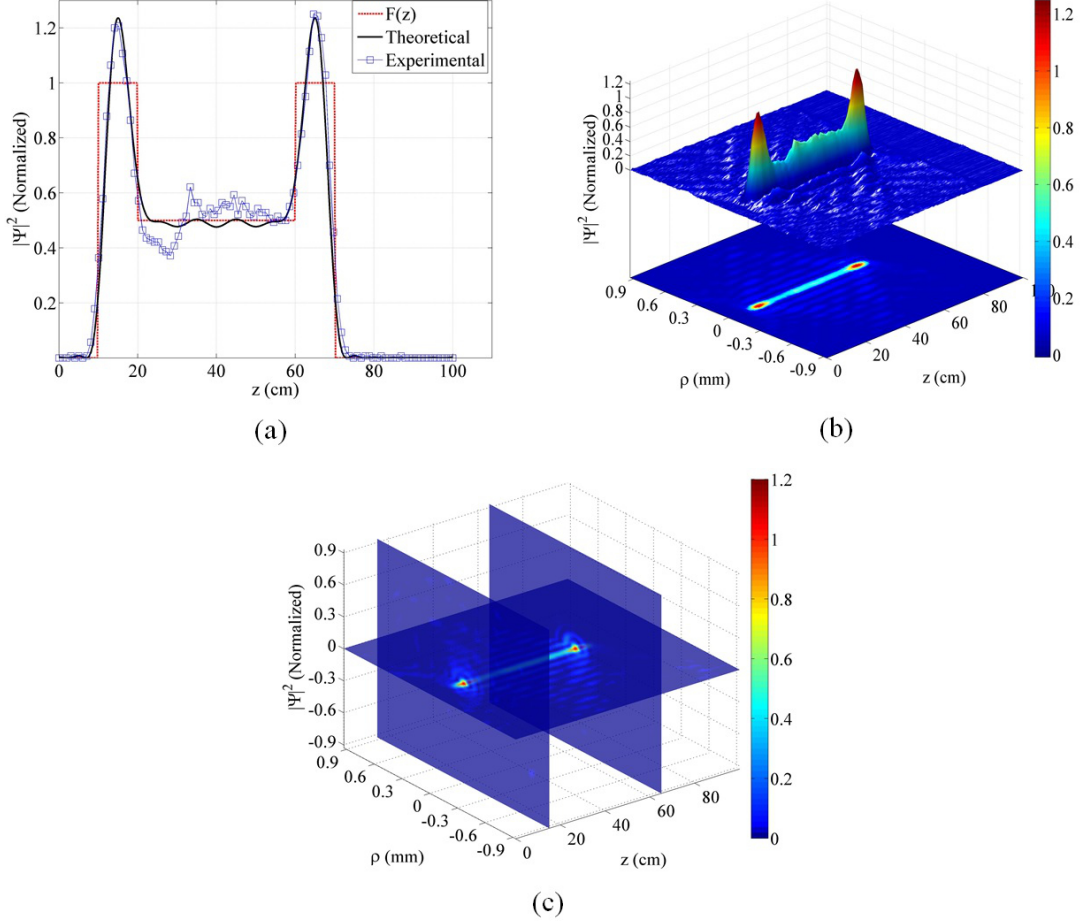


Figure 6: (a) Comparison among the longitudinal (on-axis) intensity patterns: $|F(z)|^2$, with $F(z)$ given by Eq.13, and the respective theoretical and experimental FWs; (b) Three-dimensional and projected shapes of the experimental FW; (c) Intensity pattern slices of the experimental FW.

Fifth example:

As we already said, it is possible to generate FWs with higher-order Bessel beams ($\nu > 0$ in solution (1)). In these cases, the desired longitudinal intensity pattern is shifted from the axis ($\rho = 0$) to a cylindrical surface, whose radius may be approximately calculated using (6). For details the reader is invited to consult the references [1, 2, 3, 4].

In this example we choose a longitudinal intensity pattern given by an exponential function of increasing intensity along the propagation direction, more specifically we

choose:

$$F(z) = \begin{cases} \exp(qz);, & \text{for } l_1 < z < l_2 \\ 0, & \text{elsewhere} \end{cases} \quad (14)$$

with $q = 4/7$ ($l_1 = 10\text{cm}$, $l_2 = 50\text{cm}$)

Now, instead of using zero-order Bessel beams in the solution (1), we will use $\nu = 2$ (second-order Bessel beams). Remembering that we use the solution (1) with k_{zn} and A_n given by Eqs. (3) and (5), and that (in the first five examples) we adopted $Q = 0.9999943k$, $N = 9$ and $L = 100\text{cm}$.

Figure 7 shows the 3D intensity of the experimental FW. We can easily see that the desired intensity pattern occurs on a cylindrical surface.

There is an excellent agreement between theory and experiment.

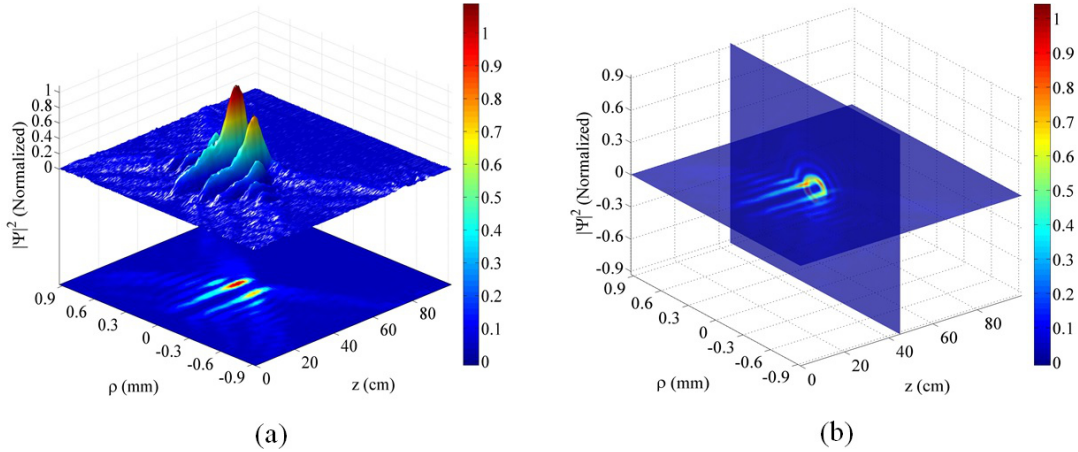


Figure 7: (a) Intensity pattern of experimental result of the chosen $|F(z)|^2$, with $F(z)$ given by Eq.(14); (b) Intensity pattern slices of the experimental FW.

Sixth example:

Finally the last two examples was made in reflective SLM Setup 2, in this case due large bandwidth we choice $Q = 0.99996k$, and from Eq.9 $N_{max} = 24.02$, if we choose $N = 24$, we find the maximum possible value of the wave number transverse in Bessel beams superpositions $k_{\rho n=N} = 12.5 \times 10^4 m^{-1}$. In this case we have $k_{\rho n=0} = 8.88 \times 10^4 m^{-1}$, which implies in a spot of radius $\Delta\rho_0 = 27 \mu m$ to the resulting FW.

So for $F(z)$ given by Eq.15,

$$F(z) = \begin{cases} \frac{-4(z^2 - z(l_2 + l_1) + l_1 l_2)}{(l_2 - l_1)^2}; & \text{for } l_1 < z < l_2 \\ \exp(qz); & \text{for } l_3 < z < l_4 \\ 0; & \text{elsewhere} \end{cases} \quad (15)$$

where $l_1 = 5\text{cm}$, $l_2 = 10\text{cm}$, $l_3 = 15\text{cm}$, $l_4 = 30\text{cm}$. We can see in Figure 8, for $F(z)$, the theoretical prediction and the experimental results.

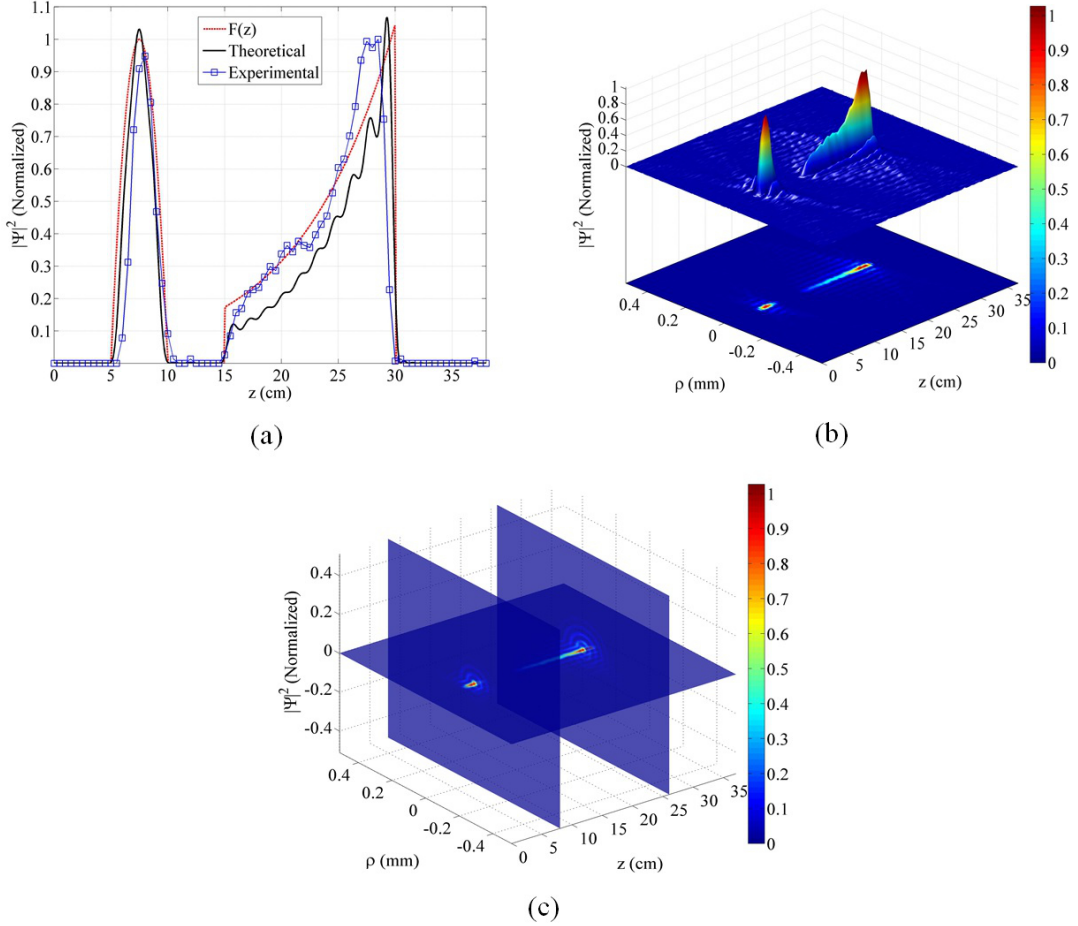


Figure 8: (a) Comparison among the longitudinal (on-axis) intensity patterns: $|F(z)|^2$, with $F(z)$ given by Eq.15, and the respective theoretical and experimental FWs; (b) Three-dimensional and projected shapes of the experimental FW; (c) Intensity pattern slices of the experimental FW.

Seventh example:

To generate a FW with the desired longitudinal intensity pattern concentrated over a cylindrical surface, we choose $F(z)$ given by Eq.(16), with $\nu = 3$ in Eq.(1), i.e. we use an higher order Bessel beam superposition.

$$F(z) = \begin{cases} 1, & \text{for } l_1 < z < l_2 \\ 0, & \text{elsewhere} \end{cases} \quad (16)$$

where, $l_1 = 15\text{cm}$, $l_2 = 25\text{cm}$.

The results are show in Figure 9, this pattern can be used to many applications as wave or atoms guide [16, 7, 17].

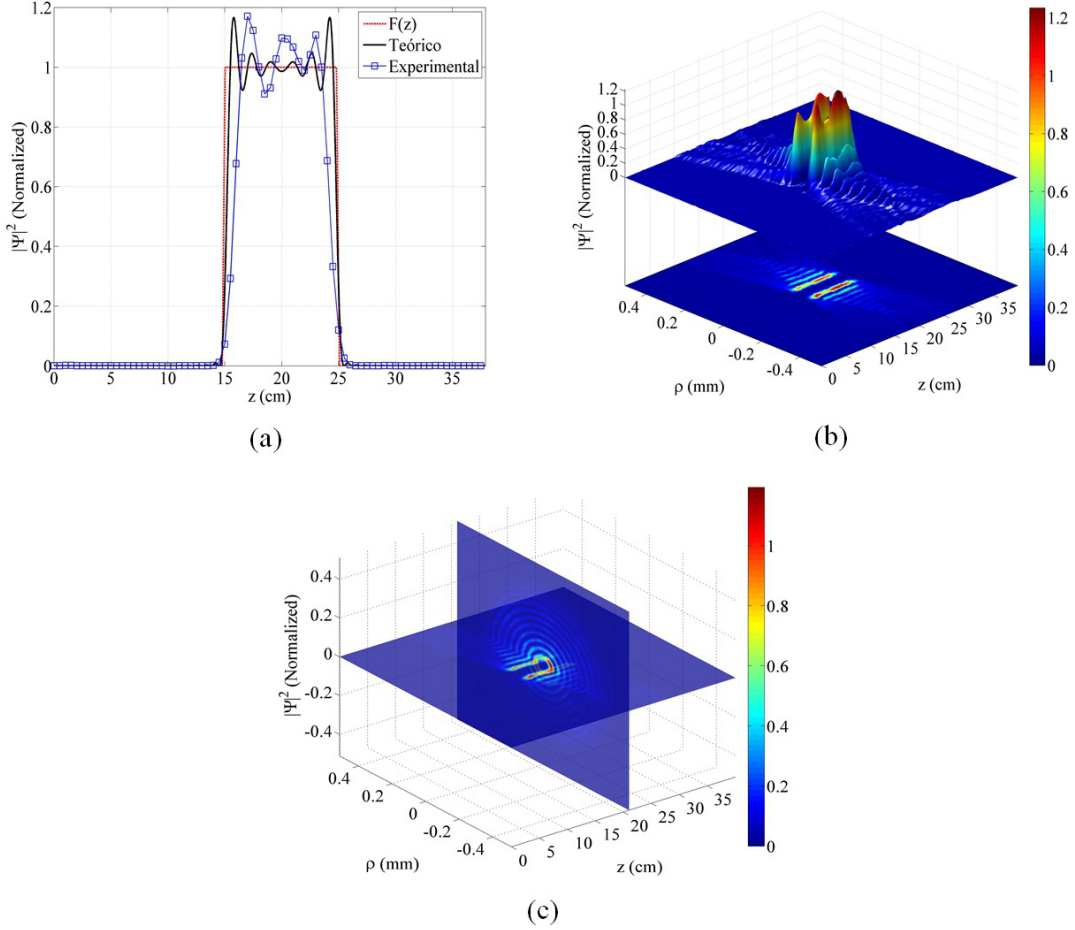


Figure 9: (a) Comparison among the longitudinal (on-axis) intensity patterns: $|F(z)|^2$, with $F(z)$ given by Eq.16, and the respective theoretical and experimental FWs; (b) Three-dimensional and projected shapes of the experimental FW; (c) Intensity pattern slices of the experimental FW.

4 Conclusions

The so called Frozen Waves are nondiffracting beams whose longitudinal (and, to lesser extent, also the transverse) intensity pattern can be freely chosen a priori. In this paper,

we present the experimental generation of several Frozen Waves via computer generated holograms implemented in two types of spatial light modulators, transmission and reflective. The experimental results for all FWs here considered are in excellent agreement with theoretical predictions. This fact opens interesting possibilities for applying these and many other FWs to scientific and technological purposes such as optical tweezers, remote sensing, atom guides, optical scalpels or acoustic, electromagnetic or ultrasound of high intensity in medicine, among others.

5 Acknowledgements

The authors are grateful to Erasmo Recami and Mikiya Muramatsu for many stimulating contacts and discussions.

The authors acknowledge partial support from UFABC, UNICAMP, CAPES, FAPESP (grants 09/11429-2 and 11/51200-4) and CNPQ (grants 307962/2010-5 and 309911/2011-7).

References

- [1] Michel Zamboni-Rached: “Stationary optical wave fields with arbitrary longitudinal shape by superposing equal frequency Bessel beams: Frozen Waves”, *Opt. Express* 17 (2004) 4001-4006.
- [2] Michel Zamboni-Rached and Erasmo Recami and Hugo E. Hernández-Figueroa: “Theory of “frozen waves”: modeling the shape of stationary wave fields”, *J. Opt. Soc. Am. A* 11 (2005) 2465-2475.
- [3] Michel Zamboni-Rached: “Diffraction-Attenuation resistant beams in absorbing media”, *Opt. Express* 14 (2006) 1804.
- [4] Michel Zamboni-Rached and Leonardo A. Ambrósio and Hugo E. Hernández-Figueroa: “Diffraction–attenuation resistant beams: their higher-order versions and finite-aperture generations”, *Appl. Opt.* 49 (2010) 5861.

- [5] S Zwick and T Haist and Y Miyamoto and L He and M Warber and A Hermerschmidt and W Osten: “Holographic twin traps”, *J. App. Opt. A: Pure and Applied* 11 (2009) 034011.
- [6] Ronald E. Meyers and Keith S. Deacon and Arnold D. Tunick and Yanhua Shih: “Virtual ghost imaging through turbulence and obscurants using Bessel beam illumination”, *Appl. Phys. Lett.* 100 (2012) 061126.
- [7] Chu, Steven and Bjorkholm, J. E. and Ashkin, A. and Cable, A: “Experimental Observation of Optically Trapped Atoms”, *Phys. Rev. Lett.* 57 (1986) 314-317.
- [8] Tarcio A. Vieira and Marcos R. R. Gesualdi and Michel Zamboni-Rached: “Frozen waves: experimental generation”, *Opt. Lett.* 37 (2012) 2034-2036.
- [9] A. Vasara and J. Turunen and A. T. Friberg: “Realization of general nondiffracting beams with computer-generated holograms”, *J. Opt. Soc. of Am - A* 6 (1989) 1748-1754.
- [10] Zdeněk Bouchal: “Controlled spatial shaping of nondiffracting patterns and arrays”, *Opt. Lett.* 27 (2002) 1376-1378.
- [11] Victor Arrizón: “Computer holography; Liquid-crystal devices; Spatial light modulators”, *Opt. Lett.* 28 (2003) 2521-2523.
- [12] Victor Arrizón and Guadalupe Méndez and David Sánchez-de-La-Llave: “Accurate encoding of arbitrary complex fields with amplitude-only liquid crystal spatial light modulators”, *Opt. Express* 13 (2005) 7913–7927.
- [13] Judit Reményi and Péter Várhegyi and László Domján and Pál Koppa and Emőke Lőrincz: “Amplitude, Phase, and Hybrid Ternary Modulation Modes of a Twisted-Nematic Liquid-Crystal Display at 400 nm”, *Appl. Opt.* 42 (2003) 3428-3434.
- [14] Josep Nicolás and Juan Campos and María J. Yzuel: “Phase and amplitude modulation of elliptic polarization states by nonabsorbing anisotropic elements: application to liquid-crystal devices”, *J. Opt. Soc. Am. A* 19 (2002) 1013–1020.

- [15] J.W.Goodman: *Introduction to Fourier Optics* (McGraw-Hill, 1996).
- [16] Song Lan and Charalambos Anastassiou and Mordechai Segev and Ming-feng Shih and J. A. Giordmaine and Greg Mizell: “Tuning of second-harmonic generation in waveguides induced by photorefractive spatial solitons”, *Applied Physics Letters* 77 (2000) 2101-2103.
- [17] Y. Song and D. Milam and W. T. Hill III: “Long, narrow all-light atom guide”, *Opt. Lett.* 24 (1999) 1805–1807.